

Native point defects in yttria and relevance to its use as a high-dielectric-constant gate oxide material: First-principles study

J. X. Zheng,¹ G. Ceder,^{1,2} T. Maxisch,² W. K. Chim,^{1,3} and W. K. Choi^{1,3}

¹Singapore-MIT Alliance, 4 Engineering Drive 3, Singapore 117576

²Department of Materials Science and Engineering, Massachusetts Institute of Technology, 77 Massachusetts Avenue, Cambridge, Massachusetts 02139-66307, USA

³Department of Electrical & Computer Engineering, National University of Singapore, 4 Engineering Drive 3, Singapore 117576

(Received 13 December 2005; published 3 March 2006)

Yttria (Y_2O_3) has become a promising gate oxide material to replace silicon dioxide in metal-oxide-semiconductor devices. Using a first-principles approach the electronic structure, defect structure, and formation energy of native point defects in Y_2O_3 are studied. Vacancies, interstitials, and antisites in their relevant charge states are considered. We find that within the band gap of Y_2O_3 oxygen vacancies, oxygen interstitials, yttrium vacancies, and yttrium interstitials can be stable depending on the Fermi level and external chemical potentials. When the Fermi level is constrained to be within the band gap of silicon, oxygen vacancies are the dominant defect type under low oxygen chemical potential condition. A higher oxygen chemical potential leads to oxygen interstitials and ultimately yttrium vacancies.

DOI: [10.1103/PhysRevB.73.104101](https://doi.org/10.1103/PhysRevB.73.104101)

PACS number(s): 77.84.-s, 74.62.Dh, 71.20.Ps

I. INTRODUCTION

Yttrium oxide (Y_2O_3) is widely used in ceramic and glass applications as it has a high melting point, high breakdown strength, and good chemical stability. Y_2O_3 is also an important oxide-based phosphor material and is used as a host material in rare-earth-doped lasers. Recently, Y_2O_3 has received attention as a promising candidate for replacing silicon dioxide (SiO_2) as a gate dielectric material in metal-oxide-semiconductor (MOS) transistors.¹⁻¹⁰ The continual scaling of complementary MOS technologies has pushed SiO_2 gate oxide to its minimal thickness limit. Y_2O_3 has emerged as a promising oxide with a moderately high dielectric constant (~ 16), relatively high band offsets with respect to silicon, and good thermodynamic stability in contact with silicon (Si). Y_2O_3 is also one of the few high dielectric constant (high- k) oxides that is epitaxially matched to Si, as its lattice constant (10.6 Å) is about two times that of Si (5.43 Å). This property of Y_2O_3 suggests that a sharp Y_2O_3 /Si interface with low interface trap density can potentially be obtained.

Although many experimental groups have studied the structural and electrical properties of the Y_2O_3 /Si system,⁴⁻¹⁰ epitaxial Y_2O_3 films do not yet have good structural and electrical quality. One major problem is the poor electrical characteristics of the interface between the high- k dielectrics and the silicon substrate. Another problem is the high density of preexisting defects in the dielectric. These defects generate positive fixed charge which shift the flat-band voltage, and electron traps which cause threshold voltage instabilities.⁸⁻¹⁰

The structural and electronic properties of stoichiometric Y_2O_3 have been studied theoretically in Refs. 11–14 and the effect of neutral oxygen vacancies on the electronic structure of Y_2O_3 was investigated by Jollet *et al.*¹² However, a detailed theoretical study of the intrinsic point defects in Y_2O_3 is lacking. In this study, we investigate the native point de-

fects in bulk yttria through first-principles calculation by calculating the formation energy of various point defects as a function of Fermi level and yttrium (Y) or oxygen (O) chemical potential.

II. COMPUTATIONAL METHODOLOGY

A. Methodology

Calculations have been performed using the generalized gradient approximation (GGA) with the Perdew-Wang exchange correlation potential³⁸ within the framework of density functional theory (DFT), as implemented in the VASP program (Vienna *ab-initio* simulation package).¹⁵ Projector augmented wave (PAW) pseudopotentials^{16,39} that were generated in the $4s^2 4p^6 5s^2 4d^1$ configuration for yttrium and the $2s^2 2p^4$ configuration for oxygen were used for all calculations. The primitive cell of Y_2O_3 consists of 40 atoms, but a cubic bixbyite structure with 80 atoms is used to compute defect states. Two inequivalent cation sites exist: Y1 at the $8b$ site [at position $(\frac{1}{4}, \frac{1}{4}, \frac{1}{4})$] and Y2 at the $24d$ site [at position $(u, 0, \frac{1}{4})$], and one type of O at the $48e$ site [at position (x, y, z)]. The perfect structure is defined by the lattice parameter a and by the four internal structural parameters u , x , y , and z .

The formation energy of point defects that do not preserve the Y_2O_3 stoichiometry depends on the external chemical potentials. We follow the standard formalism outlined in several previous studies¹⁷⁻²³ to define reasonable bounds on the chemical potentials and to investigate the defect energies within these limits. The Y and O chemical potentials are not independent but related to the total energy of Y_2O_3 :

$$2\mu_Y^{Y_2O_3} + 3\mu_O^{Y_2O_3} = E_{Y_2O_3}, \quad (1)$$

where $\mu_Y^{Y_2O_3}$ and $\mu_O^{Y_2O_3}$ are the chemical potentials of Y and O in Y_2O_3 , respectively, and $E_{Y_2O_3}$ is the energy per molecule of pure Y_2O_3 . The Y_2O_3 compound can exist within a

range of oxygen and yttrium chemical potentials, defined by the competing phases at other Y/O ratios. The largest possible range for μ_{O} and μ_{Y} is obtained from the stability limits of Y_2O_3 with respect to metallic yttrium and molecular oxygen. To prevent pure Y formation, the following condition needs to be fulfilled:

$$\mu_{\text{Y}}^{\text{Y}_2\text{O}_3} < \mu_{\text{Y}}^{\circ}, \quad (2)$$

where $\mu_{\text{Y}}^{\text{Y}_2\text{O}_3}$ is the chemical potential of Y in Y_2O_3 and μ_{Y}° is the chemical potential of Y in pure yttrium metal.

To prevent oxygen loss, the following condition needs to be fulfilled:

$$\mu_{\text{O}}^{\text{Y}_2\text{O}_3} < \mu_{\text{O}}^{\circ}, \quad (3)$$

where $\mu_{\text{O}}^{\text{Y}_2\text{O}_3}$ is the chemical potential of O in Y_2O_3 and μ_{O}° is the energy of pure O_2 gas (per oxygen atom). These chemical potentials are related by the formation energy of Y_2O_3 from metallic Y and O_2 gas:

$$\Delta E_f^{\text{Y}_2\text{O}_3} = 2\mu_{\text{Y}}^{\text{Y}_2\text{O}_3} - 2\mu_{\text{Y}}^{\circ} + 3\mu_{\text{O}}^{\text{Y}_2\text{O}_3} - 3\mu_{\text{O}}^{\circ}. \quad (4)$$

Combining Eqs. (2)–(4), we obtain the range of $\mu_{\text{Y}}^{\text{Y}_2\text{O}_3}$ for which the defect energies should be evaluated:

$$\mu_{\text{Y}}^{\circ} + \frac{1}{2}\Delta E_f^{\text{Y}_2\text{O}_3} < \mu_{\text{Y}}^{\text{Y}_2\text{O}_3} < \mu_{\text{Y}}^{\circ}. \quad (5)$$

The range for $\mu_{\text{Y}}^{\text{Y}_2\text{O}_3}$ can be found by combining Eqs. (1) and (5).

B. Defect formation energies

The supercell approach is used to calculate defect energies in this study. A defect α in charge state q is placed in a large Y_2O_3 supercell which is repeated periodically. To calculate the formation energy of charged defects, a neutralizing background charge is applied. The formation energy (E_f) of a charged point defect [α^q] in Y_2O_3 is computed as

$$E_f[\alpha^q] = E[\alpha^q] \pm \mu_X - E[\text{bulk}] + q(E_V + \Delta V + \varepsilon_F), \quad (6)$$

where $E[\alpha^q]$ is the total energy of a supercell containing a point defect α with charge q , μ_X is the external chemical potential of element X with a + sign for vacancy and a – sign for interstitial defect, $E[\text{bulk}]$ is the total energy of a perfect supercell, and E_V is the valence band maximum (VBM) in the perfect supercell. The Fermi level is taken as the energy of the electron reservoir (electron chemical potential μ_e) from (in) which an electron is removed (placed) to form a charged defect. The Fermi level is conventionally taken to be zero at the VBM of the perfect supercell. Because the valence band is displaced in calculations on small supercells with defects, its value needs to be referenced back to the valence band in the perfect crystal by an amount ΔV .^{19–23} The shift of the VBM in supercell calculations, ΔV , can be obtained from the difference between the average electrostatic potential in a bulklike environment of the defect supercell and the average electrostatic potential in the perfect bulk supercell. To calculate the average electrostatic potential, the macroscopic averaging technique^{24,25} is used to find the shift in the VBM. The three-dimensional electrostatic potential is

reduced to a one-dimensional planar average first, and the macroscopic average is calculated over the primitive cell along one direction.

For charged systems, the energy of charged defects converges very slowly with supercell size due to electrostatic interactions between the defects across the periodic boundary conditions. This interaction scales as $1/\varepsilon L$, where L is the linear dimension of supercell and ε is the dielectric constant.²⁶ To achieve faster convergence, Makov and Payne²⁶ suggested adding correction terms to the energy to account for defect-defect interactions induced by the periodic boundary conditions. Although this approach works well for atomic or molecular systems, it may lead to an overestimation of the correction term for defects in semiconductors due to the increased screening from valence electrons which effectively reduce the strength of the interactions.^{23,27,28} For this reason, we have not included these correction terms in this study.

Errors in the defect formation energy can come from various sources. Well-converged calculations reduce the error from plane-wave energy cutoff and k -point sampling below 10 meV. The interaction between charged defects can introduce an error on the order of 0.1 eV and this error may become larger for higher-charged defects. The band gap error due to density-functional theory itself would have a significant effect on donorlike defects and is discussed with more details in Sec. IV. In summary, a possible error for defect formation energies of a few tenths of an eV should always be assumed.

The thermodynamic transition between two charge states on the defect q_1 and q_2 occurs for the Fermi level at which the formation energy of [q_1] is equal to that of [q_2], i.e., $E_f[q_1] = E_f[q_2]$. Using Eq. (6), it can be shown that the thermodynamic transition level q_1/q_2 is

$$\varepsilon_F[q_1/q_2] = \frac{1}{q_2 - q_1} (E[q_1] - E[q_2] + q_1(E_V + \Delta V_1) - q_2(E_V + \Delta V_2)), \quad (7)$$

where q_1 and q_2 are the initial and final charge states, respectively (including the signs), ΔV_1 and ΔV_2 are the VBM shift for the initial and final charge states, respectively, and $\varepsilon_F[q_1/q_2]$ is the Fermi energy level at which the transition from q_1 to q_2 takes place. This thermodynamic transition level can be directly observed in deep-level transient spectroscopy experiments.

III. RESULTS

A. Perfect-Crystal Y_2O_3

The pseudopotentials have been validated on bulk yttria. Convergence of the total energy to within 10 meV was achieved with a 500 eV cutoff energy for plane wave basis and a Monkhorst-Pack k -point grid of $2 \times 2 \times 2$ for Brillouin zone integration. The calculated parameters, along with experimental values, are shown in Table I. The bulk modulus (B) is obtained by fitting the energy versus volume curve using a fourth-order polynomial.

TABLE I. Calculated and experimental unit cell parameters and bulk modulus of yttria.

Reference		u	x	y	z	a	B (GPa)
29	exp	-0.0314	0.389	0.150	0.377	10.604	
30	exp	-0.0323	0.391	0.150	0.383		
31	exp						150
32	LDA	-0.0326	0.3907	0.1514	0.3797	10.515	
32	GGA	-0.0327	0.3908	0.1516	0.3799	10.700	
Present work	GGA	-0.0324	0.3908	0.1515	0.3798	10.700	150

The total electron density of states (DOS), as well as their atomic and orbital projected DOS, are shown in Fig. 1. It can be seen that a valence band (VB3) of yttrium $4p$ is centered around -20 eV, a valence band (VB2) of oxygen $2s$ is centered around -15 eV, a valence band (VB1) of oxygen $2p$ occurs below 0 eV, and a conduction band (CB) of yttrium $4d$ occurs above 4.1 eV. There is a small intermixing of Y $4d$ and O $2p$ states in the valence band near 0 eV, which is consistent with the limited covalent bonding between Y and O atoms. The calculated band gap is about 4.1 eV, which is smaller than the experimental value³³ of 6 eV. The underestimation of the band gap energy value is typical of DFT calculations in the GGA or LDA approximations.

B. Defect formation energies

Yttrium metal has a hexagonal close-packed structure. Using a $20 \times 20 \times 20$ uniform k -space mesh, we calculate equilibrium lattice parameters of $a=3.63$ Å (3.65 Å) and $c=5.70$ Å (5.73 Å). Values in parenthesis are experimental data from Ref. 29. The energy of O_2 was calculated from a single molecule in a 10 Å cubic cell. While the calculated formation energy for Y_2O_3 of -19.41 eV/ Y_2O_3 is close to the experimental enthalpy of formation³⁴ of

-19.62 eV/ Y_2O_3 , this result may be fortuitous given the known problem in calculating the O_2 binding energy.^{35,36}

The energy to form a yttrium vacancy on the Y1 site is about 0.2 eV lower than on the Y2 site; thus only Y1 vacancy formation energies are reported. There are two interstitial sites, $8a$ and $16c$, in yttria. The interstitial site at $8a$ is octahedrally coordinated, surrounded by six oxygen atoms and six yttrium atoms. The interstitial site at $16c$ is surrounded by four yttrium atoms and six oxygen atoms and filling it with oxygen would lead to a fluorite structure. The formation energies for interstitials (both oxygen and yttrium) at $8a$ are always 0.4 – 1.2 eV higher than interstitials at the $16c$ site. Hence only formation energies for interstitials at $16c$ are reported. For oxygen antisites, the oxygen at Y2 has 2 to 3 eV lower energy than the oxygen at Y1; thus the formation energies for oxygen at Y2 site are reported. The formation energy of these defects in various charge states and at the different extremes of chemical potentials and Fermi levels are given in Table II.

The lower limit for the Fermi level ($\epsilon_F=0$ eV) corresponds to the top of the valence band while the upper limit ($\epsilon_F=6$ eV) represents the bottom of the experimental conduction band. The formation energies for different defects as a function of Fermi level for the two limiting yttrium chemical potentials and one intermediate yttrium chemical potential are shown in Fig. 2. The slope of the lines in these figures corresponds to the charge state of the defect. For each defect, the line for a particular charge state has only been drawn over the range where this charge state has the lowest energy of all possible charge states. The changes of slope in the curves correspond to the transitions between charge states (and hence to thermodynamic defect energy levels).

C. Defect structure

The results from our calculations suggest that the most common native point defects are oxygen vacancies (V_O), oxygen interstitials (O_i), and yttrium vacancies (V_Y). A summary of relaxed local bond lengths for these defect types is shown in Table III. The changes in bond lengths for each defect can be understood in terms of ionic size and charge effects. When an oxygen atom is removed, the nearest yttrium atoms move slightly away from the vacancy site as they are no longer electrostatically attracted to it, and oxygen atoms move closer to the vacancy site as the electrostatic

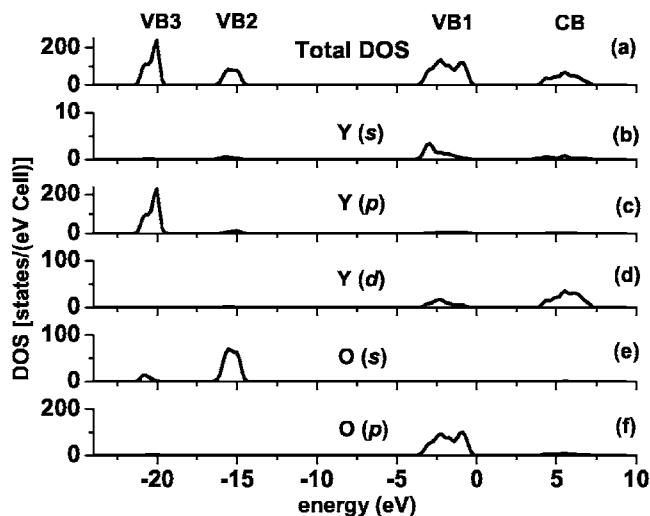


FIG. 1. (a) Total DOS of Y_2O_3 , (b) Y s -orbital projected DOS, (c) Y p -orbital projected DOS, (d) Y d -orbital projected DOS, (e) O s -orbital projected DOS, and (f) O p -orbital projected DOS.

TABLE II. Point defect formation energies (E_f) in Y_2O_3 .

Defect	Defect site	Charge on defect	Kröger-Vink notation	$E_f(\mu_Y = \mu_Y^0)$ (eV)		$E_f(\mu_Y = \mu_Y^0 + \frac{1}{2}\Delta E_f^{Y_2O_3})$ (eV)	
				$\epsilon_F = 0$ eV	$\epsilon_F = 6$ eV	$\epsilon_F = 0$ eV	$\epsilon_F = 6$ eV
V_O	e	0	V_O^X	0.45	0.45	6.92	6.92
V_O	e	+1	V_O'	-2.46	3.54	4.01	10.01
V_O	e	+2	V_O''	-5.21	6.79	1.25	13.25
V_Y	b	0	V_Y^X	13.52	13.52	3.82	3.82
V_Y	b	-1	V_Y'	13.59	7.59	3.89	-2.11
V_Y	b	-2	V_Y''	13.75	1.75	4.05	-7.95
V_Y	b	-3	V_Y'''	14.07	-3.93	4.37	-13.63
O_i	c	0	O_i^X	7.85	7.85	1.38	1.38
O_i	c	-1	O_i'	8.01	2.01	1.54	-4.46
O_i	c	-2	O_i''	8.38	-3.62	1.91	-10.09
Y_i	c	0	Y_i^X	4.78	4.78	14.48	14.48
Y_i	c	+1	Y_i'	0.63	6.63	10.33	16.33
Y_i	c	+2	Y_i''	-2.98	9.02	6.72	18.72
Y_i	c	+3	Y_i'''	-6.58	11.42	3.11	21.11
Y_O	e	0	Y_O^X	6.03	6.03	22.20	22.20
Y_O	e	+1	Y_O'	1.94	7.94	18.10	24.10
Y_O	e	+2	Y_O''	-1.98	10.02	14.19	26.19
Y_O	e	+3	Y_O'''	-6.34	11.66	9.82	27.82
O_Y	d	0	O_Y^X	18.37	18.37	2.20	2.20
O_Y	d	-1	O_Y'	19.27	13.27	3.10	-2.90
O_Y	d	-2	O_Y''	21.22	9.22	5.05	-6.95

repulsion is reduced. This is different from what is found for oxygen vacancies in ZnO (Ref. 17) in which nearest zinc atoms move closer to an oxygen vacancy. Near a yttrium vacancy, oxygen atoms move farther away from the vacancy site while yttrium atoms move slightly closer to the vacancy site. This is similar to what was observed for zinc vacancies in ZnO.¹⁷ For the oxygen interstitial, the neighboring yttrium atoms move closer to the interstitial site since they are electrostatically attracted, and the neighboring oxygen atoms move away from the interstitial site due to the electrostatic repulsion from the interstitial oxygen.

IV. DISCUSSION

Under high yttrium partial pressure (or low oxygen partial pressure) [Fig. 2(a)], Y_i and V_O are competing defects when the Fermi level is close to the VBM of Y_2O_3 . As the Fermi level moves up, V_O becomes dominant due to its lower positive charge, and finally O_i dominates when the Fermi level is close to the CBM. Lowering the yttrium partial pressure reduces the stability of the yttrium interstitial so that even for a low Fermi level it is not stable anymore. For the intermediate chemical potentials as shown in Fig. 2(b), V_O is stable at low Fermi level. At higher Fermi level, the oxygen interstitial is stabilized because of its higher number of electrons. Only for Fermi levels very close to the conduction band is the yttrium

vacancy lowest in energy. Under low yttrium partial pressure [Fig. 2(c)], O_i dominates when the Fermi level is close to the VBM and V_Y dominates when the Fermi level is close to the CBM. Hence in general we observe that the Fermi level has a strong influence on which defect can be found. When the Fermi level is near the VBM defects with a low number of electrons are stable, such as the oxygen vacancy or the yttrium interstitial. High electron count defects such as the oxygen interstitial or yttrium vacancy are found for higher Fermi level. Whether an O-rich (O_i or V_Y) or Y-rich (V_O or Y_i) defect situation occurs depends then on the external chemical potential.

The transition Fermi levels for the dominant defect types, V_O , O_i , V_Y , and Y_i , are shown in Fig. 3, within the calculated band gap. The transition energies for both oxygen interstitial (O_i) and yttrium vacancy (V_Y) are very close to the VBM of Y_2O_3 , while the transitions for the oxygen vacancy (V_O) are located ~ 1.2 – 1.4 eV below the calculated CBM. The yttrium interstitial (Y_i) levels are located about 0.5 eV below the CBM.

As the band gap of Y_2O_3 is underestimated by 1.9 eV in GGA, it is important to estimate how the thermodynamic transition levels shown in Fig. 3 would change with a more accurate band gap. One common method^{17,23,37} to include corrections to the band gap is to leave the energy levels of the acceptorlike defects near the VBM unchanged, but let the

TABLE III. Distances to nearest-neighbor atoms for bulk and defect sites in Y_2O_3 . d_i is the distance of the i th nearest neighbor in angstroms. The values in parentheses are the number of neighbors having the same distance.

	Neighbor type	d_1	d_2	d_3	d_4
O (in bulk Y_2O_3)	Y	2.27(1)	2.29(1)	2.30(1)	2.36(1)
	O	2.94(2)	2.95(2)		
Neutral V_O	Y	2.29(1)	2.35(1)	2.36(1)	2.39(1)
	O	2.903(1)	2.907(1)	2.91(1)	2.92(1)
Y (in bulk Y_2O_3)	Y	3.55(6)			
	O	2.30(6)			
Neutral V_Y	Y	3.53(6)			
	O	2.61(6)			
O (before relaxation)	Y	2.47(3)	2.50(1)		
	O	2.43(3)	2.50(3)		
Neutral O_i	Y	2.30(1)	2.34(3)		
	O	2.61(3)	2.65(3)		

mediate yttrium chemical potential [Fig. 2(b)], charged oxygen interstitials become dominant. Under low yttrium chemical potential (or high oxygen partial pressure) [Fig. 2(c)], charged yttrium vacancies are dominant. The defect levels from oxygen interstitials and yttrium vacancies are close to the VBM of Y_2O_3 and will be negatively charged in most of the range of the electron chemical potential. Thus they will only contribute to the negative fixed charge. However, the defect levels from oxygen vacancies will move upwards when a band gap correction is applied. They may become positively charged and act as electron traps. Experiments have shown the existence of defects generating positive fixed charge and electron traps in the Y_2O_3 films.⁸⁻¹⁰ The positive fixed charge will shift the flatband voltage while the electron traps can cause threshold voltage instabilities. Based on our results, we propose that Y_2O_3 films should be grown under high to intermediate oxygen partial pressure to suppress the oxygen vacancy formation.

V. CONCLUSIONS

A first-principles study of point defects in Y_2O_3 has been carried out. The stable defects can be oxygen vacancies, oxy-

gen interstitials, yttrium vacancies, and yttrium interstitials depending on the Fermi level and external chemical potentials. When the Fermi level is constrained to be within the band gap of silicon, oxygen vacancies are the dominant defect types under low oxygen chemical potential condition. A higher oxygen chemical potential leads to oxygen interstitials and ultimately yttrium vacancies. The oxygen vacancies have transition levels near the conduction band and may be responsible for the positive fixed charges and electron traps observed in experiments. We propose that Y_2O_3 films should be grown under high to intermediate oxygen partial pressure to suppress the oxygen vacancy formation.

ACKNOWLEDGMENTS

The authors would like to thank the Singapore-MIT Alliance and the National University of Singapore for supporting this work. T. Maxisch acknowledges the support by the Department of Energy under Contract No. DE-FG02-96ER45571 and by the MRSEC program of the National Science Foundation under Contract No. DMR-0213282. Additional computing resources were provided by the National Science Foundation, National Partnership for Advanced Computing Infrastructure (NPACI).

¹R. McKee, F. Walker, and M. Chisholm, *Mater. Res. Soc. Symp. Proc.* **567**, 415 (1999).

²G. D. Wilk, R. M. Wallace, and J. M. Anthony, *J. Appl. Phys.* **89**, 5243 (2001).

³E. P. Gusev, E. Cartier, D. A. Buchanan, M. Gribelyuk, M. Copel, H. Okorn-Schmidt, and C. D'Emic, *Microelectron. Eng.* **59**, 341 (2001).

⁴J. Kwo, M. Hong, A. R. Kortan, K. L. Queeney, Y. J. Chabal, J. P. Mannaerts, T. Boone, J. J. Krajewski, A. M. Sergent, and J. M. Rosamilia, *Appl. Phys. Lett.* **77**, 130 (2000).

⁵J. Kwo, M. Hong, A. R. Kortan, K. L. Queeney, Y. J. Chabal, R. L. Opila, D. A. Muller, S. N. G. Chu, B. J. Sapjeta, T. S. Lay, J. P. Mannaerts, T. Boone, H. W. Krautter, J. J. Krajewski, A. M. Sergent, and J. M. Rosamilia, *J. Appl. Phys.* **89**, 3920 (2001).

⁶S. Guha, E. Cartier, M. A. Gribelyuk, N. A. Bojarczuk, and M. C. Copel, *Appl. Phys. Lett.* **77**, 2710 (2000).

⁷L.-A. Ragnarsson, S. Guha, M. Copel, E. Cartier, N. A. Bojarczuk, and J. Karasinski, *Appl. Phys. Lett.* **78**, 4169 (2001).

⁸E. K. Evangelou, C. Wiemer, M. Fanciulli, M. Sethu, and W. Cranton, *J. Appl. Phys.* **94**, 318 (2003).

- ⁹A. C. Rastogi and S. B. Desu, *J. Electroceram.* **13**, 121 (2004).
- ¹⁰A. C. Rastogi and R. N. Sharma, *Semicond. Sci. Technol.* **16**, 641 (2001).
- ¹¹F. Jollet, C. Noguera, N. Thromat, M. Gautier, and J.-P. Duraud, *Phys. Rev. B* **42**, 7587 (1990).
- ¹²F. Jollet, C. Noguera, M. Gautier, N. Thromat, and J.-P. Duraud, *J. Am. Ceram. Soc.* **74**, 358 (1991).
- ¹³D. R. Mueller, D. L. Ederer, J. vanEk, W. L. O'Brien, Q. Y. Dong, J. J. Jia, and T. A. Callcott, *Phys. Rev. B* **54**, 15034 (1996).
- ¹⁴Y. N. Xu, Z. Q. Gu, and W. Y. Ching, *Phys. Rev. B* **56**, 14993 (1997).
- ¹⁵G. Kresse and J. Hafner, *Phys. Rev. B* **47**, R558 (1993); G. Kresse and J. Furthmüller, *ibid.* **54**, 11169 (1996); G. Kresse and J. Furthmüller, *Comput. Mater. Sci.* **6**, 15 (1996).
- ¹⁶G. Kresse and D. Joubert, *Phys. Rev. B* **59**, 1758 (1999).
- ¹⁷A. F. Kohan, G. Ceder, D. Morgan, and C. G. Van de Walle, *Phys. Rev. B* **61**, 15019 (2000).
- ¹⁸S. B. Zhang, S.-H. Wei, and A. Zunger, *Phys. Rev. B* **63**, 075205 (2001).
- ¹⁹D. B. Laks, C. G. Van de Walle, G. F. Neumark, P. E. Blöchl, and S. T. Pantelides, *Phys. Rev. B* **45**, 10965 (1992).
- ²⁰A. Garcia and J. E. Northrup, *Phys. Rev. Lett.* **74**, 1131 (1995).
- ²¹S. Poykko, M. J. Puska, and R. M. Nieminen, *Phys. Rev. B* **53**, 3813 (1996).
- ²²K. W. Kwak, D. Vanderbilt, and R. D. King-Smith, *Phys. Rev. B* **52**, 11912 (1995).
- ²³C. G. Van de Walle and J. Neugebauer, *J. Appl. Phys.* **95**, 3851 (2004).
- ²⁴A. Baldereschi, S. Baroni, and R. Resta, *Phys. Rev. Lett.* **61**, 734 (1988).
- ²⁵M. Peressi, N. Binggeli, and A. Baldereschi, *J. Phys. D* **31**, 1273 (1998).
- ²⁶G. Makov and M. C. Payne, *Phys. Rev. B* **51**, 4014 (1995).
- ²⁷C. Persson, Y. J. Zhao, S. Lany, and A. Zunger, *Phys. Rev. B* **72**, 035211 (2005).
- ²⁸J. Shim, E. K. Lee, Y. J. Lee, and R. M. Nieminen, *Phys. Rev. B* **71**, 035206 (2005).
- ²⁹R. W. G. Wyckoff, *Crystal Structures* (Wiley, New York, 1963).
- ³⁰H. Ishibashi, K. Shimomoto, and K. Nakahigashi, *J. Phys. Chem. Solids* **55**, 809 (1994).
- ³¹Ö. Ünal and M. Akinc, *J. Am. Ceram. Soc.* **79**, 805 (1996).
- ³²L. Marsella and V. Fiorentini, *Phys. Rev. B* **69**, 172103 (2004).
- ³³J. Robertson, *J. Vac. Sci. Technol. B* **18**, 1785 (2000).
- ³⁴J. G. Speight, *Lange's Handbook of Chemistry*, 16th ed. (McGraw-Hill, New York, 2005).
- ³⁵B. Hammer, L. B. Hansen, and J. K. Norskov, *Phys. Rev. B* **59**, 7413 (1999).
- ³⁶L. Wang, T. Maxisch, and G. Ceder (unpublished).
- ³⁷S. B. Zhang, S. H. Wei, A. Zunger, and H. Katayama-Yoshida, *Phys. Rev. B* **57**, 9642 (1998).
- ³⁸J. P. Perdew, J. A. Chevary, S. H. Vosko, K. A. Jackson, M. R. Perderson, D. J. Singh, and C. Fiolhais, *Phys. Rev. B* **46**, 6671 (1992).
- ³⁹P. E. Blöchl, *Phys. Rev. B* **50**, 17953 (1994).